nature biomedical engineering

Supplementary information

https://doi.org/10.1038/s41551-026-01712-9

Derivation of functional retinal endothelial cells from human pluripotent stem cells for therapeutics and modelling

In the format provided by the authors and unedited

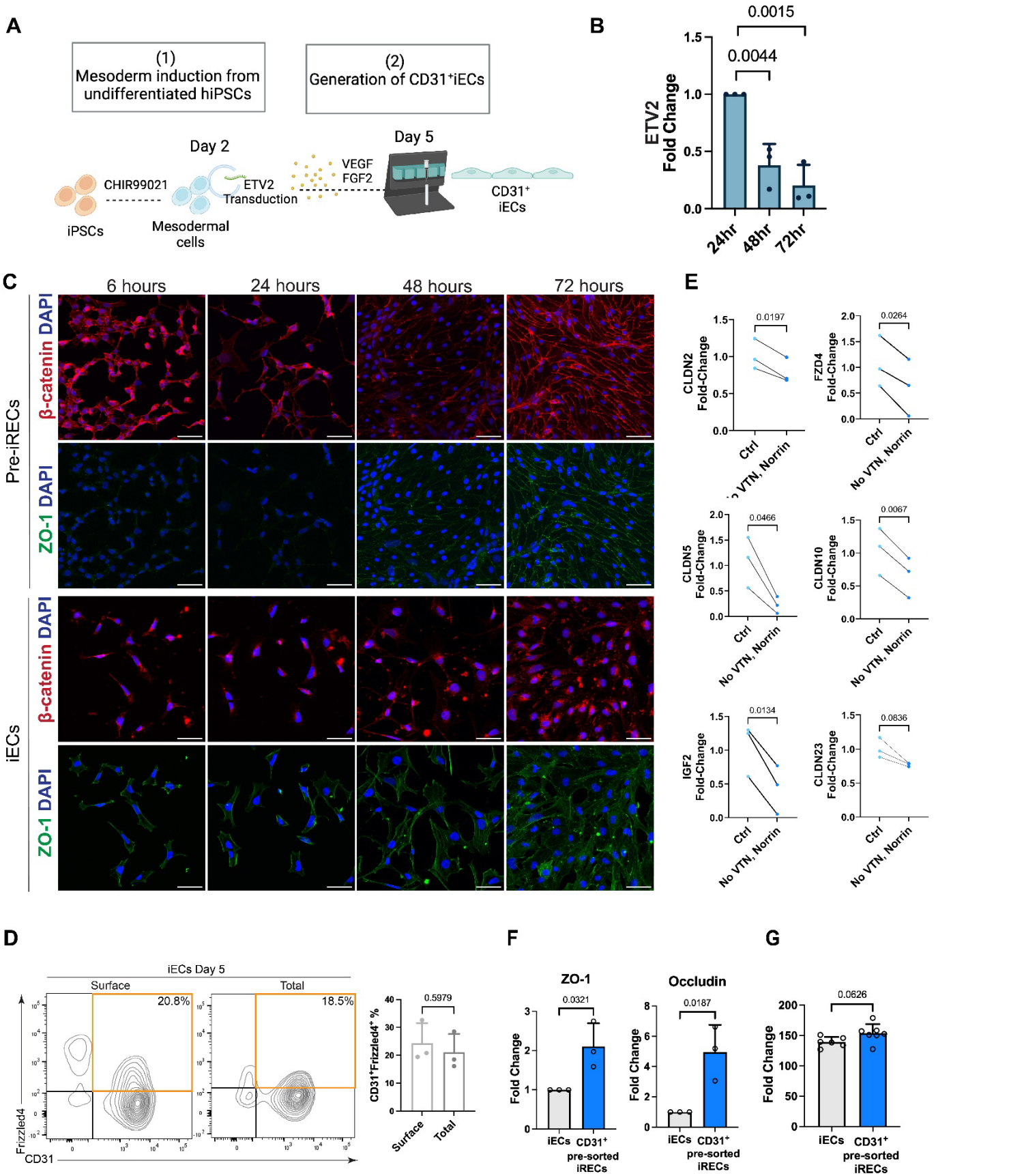

Supplementary fig 1. Generation and characterization of CD31⁺ iECs and pre-iRECs from hiPSCs.

(A) Schematic illustration of iEC differentiation. Created in BioRender. Gerecht, S. (2026) https://BioRender.com/w2co5rt. (B) RT-qPCR of ETV2 expression for pre-iRECs (N = 3 independent biological replicates, n = 3 technical replicates). (C) Representative immunofluorescence staining of β-catenin and ZO-1 proteins on pre-iRECs and iECs 6-, 24-, 48-, and 72-hours post-ETV2 electroporation. β-catenin (red), ZO-1-GFP (green), and nuclei (blue). Scale bars: 50 μm. (D) Representative flow cytometry analysis of total and surface CD31 and Frizzled4 expression on day

5 iECs (*left*) and corresponding quantification (*right*) (N = 3 independent biological replicates, n = 1 technical replicate). (E) RT-qPCR analysis of day 5 pre-iRECs differentiated with or without vitronectin (VTN) and Norrin (N = 3 independent biological replicates, n = 3 technical replicates). (F) RT-qPCR for iECs and $CD31^+$ pre-sorted iRECs on day 8. (G) TEER measurements of iECs and $CD31^+$ pre-sorted iRECs (N = 3 independent biological replicates, n = 2 technical replicates). All graphs represent means ± SD. Two-tailed paired Student t-tests were performed to statistically compare all data in Fig E. A one-factor ANOVA was used to statistically analyze Fig. B. Two-tailed unpaired Student t-tests were performed for all other statistical comparisons. Significance levels were set at $p > 0.05$, $^*p \leq 0.05$, $^{**}p \leq 0.01$, $^{***}p \leq 0.001$ and $^{****}p \leq 0.0001$. All immunofluorescence staining experiments were performed once to confirm protein expression and validated with subsequent independent experiments of iECs and iRECs.

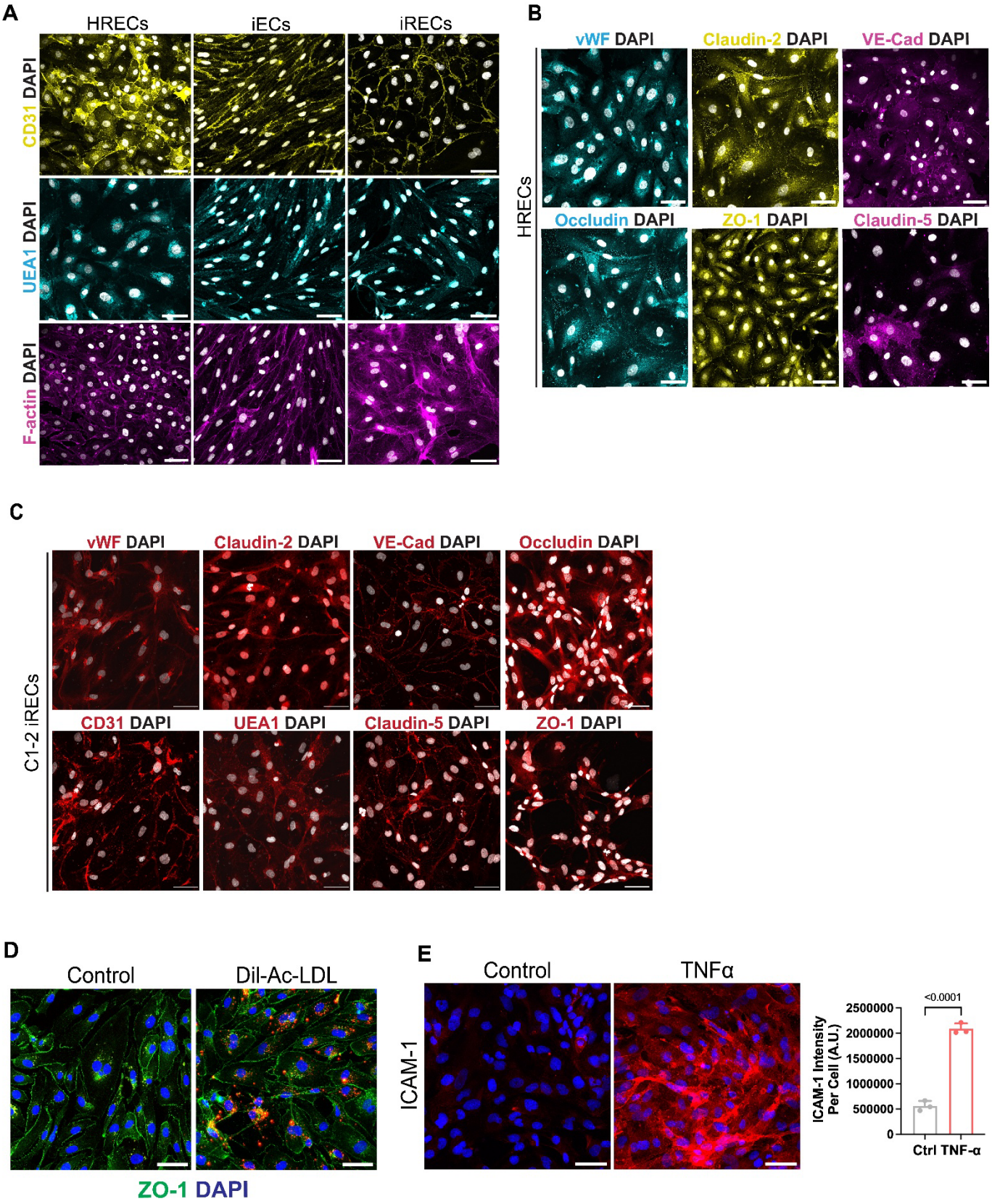

Supplementary fig 2. Proteomic characterization of HRECs, iECs, and iRECs, and functional validation of iRECs.

(A) Representative immunofluorescence images of EC markers in HRECs, iECs, and iRECs. CD31 (yellow), UEA1 (cyan), F-actin (magenta), and nuclei (white). (B) Representative immunofluorescence images of EC and junctional protein markers in HRECs. Claudin-5, and VE-Cadherin (magenta), Claudin-2 and ZO-1 (yellow), vWF and Occludin (Cyan), and nuclei (white). (C) Representative immunofluorescence images of EC, junctional, and retinal protein markers in C1-2 hiPSC-derived iRECs. vWF, Claudin-2, VE-Cad, CD31, UEA1, Claudin-5, Occludin, and ZO-1 (red) and nuclei (white). Scale bars: 50 μm. (D) Representative immunofluorescence images of Dil-Ac-

LDL (red) uptake in iRECs. ZO-1 (green) and nuclei (blue). Scale bars: 50 μm. (E) Representative immunofluorescence images and quantification of ICAM-1 (red) expression in TNFα-treated and untreated iRECs (N = 3 independent biological replicates, n = 2 technical replicates). Nuclei (blue). Scale bars: 50 μm. All graphs represent means ± SD. Two-tailed unpaired Student t-tests were performed for all statistical comparisons. Significance levels were set at $p > 0.05$, $*p \leq 0.05$, $**p \leq 0.01$, $***p \leq 0.001$ and $****p \leq 0.0001$. All Fig. E immunofluorescence staining experiments were performed with three independent biological replicates to accurately quantify associated fluorescence expression and ensure reproducibility. The other immunofluorescence staining experiments were performed once to confirm protein expression and ensure reproducibility.

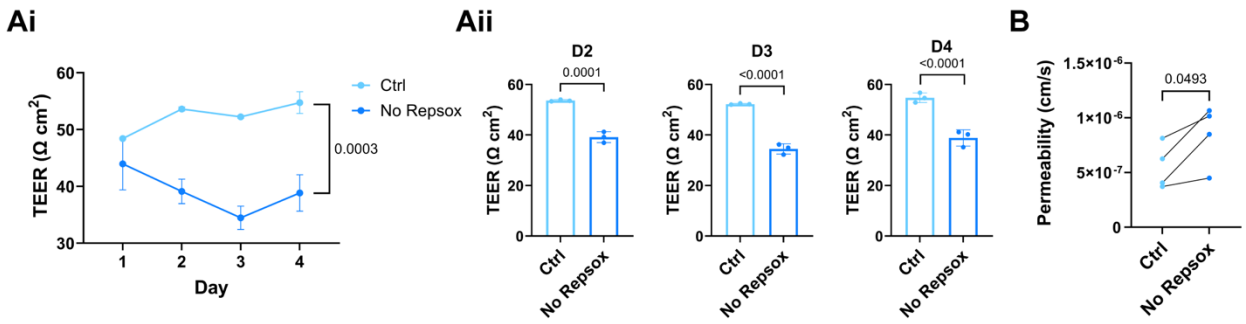

Supplementary fig 3. Barrier function analysis of iRECs treated with or without RepSox. (A) i. TEER measurement for iRECs treated with or without RepSox across the four-day culture period (N = 3 independent biological replicates, n = 3 technical replicates). ii. Post-hoc Tukey's analysis of the TEER data on day two, three, and four (N = 3 independent biological replicates, n = 3 technical replicates). (B) Permeability assay for iRECs treated with or without RepSox (N = 4 independent biological replicates, n = 3 technical replicates). All graphs represent means ± SD. For TEER assays, we utilized two-factor repeated measures ANOVA to compare cell types. Post-hoc Tukey's tests were then performed to analyze individual days. Two-tailed paired Student t-tests were performed to statistically compare permeability data. Significance levels were set at $p > 0.05$, $*p \leq 0.05$, $**p \leq 0.01$, $***p \leq 0.001$ and $****p \leq 0.0001$.

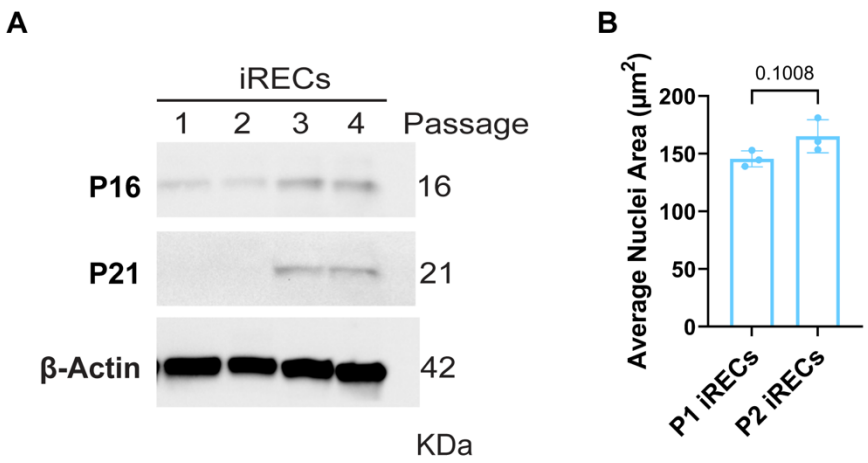

Supplementary fig 4. Senescence analysis and morphological characterization of iRECs. (A) Representative western blot for P16, P21 and β-actin of iRECs. (B) Quantification of nuclei area for passage one and two iRECs (N = 1 independent biological replicate, n = 3 technical replicates). All graphs represent means ± SD. Two-tailed unpaired Student t-tests were performed for all statistical comparisons. Significance levels were set at $p > 0.05$, $*p \leq 0.05$, $**p \leq 0.01$, $***p \leq 0.001$ and $****p \leq 0.0001$.

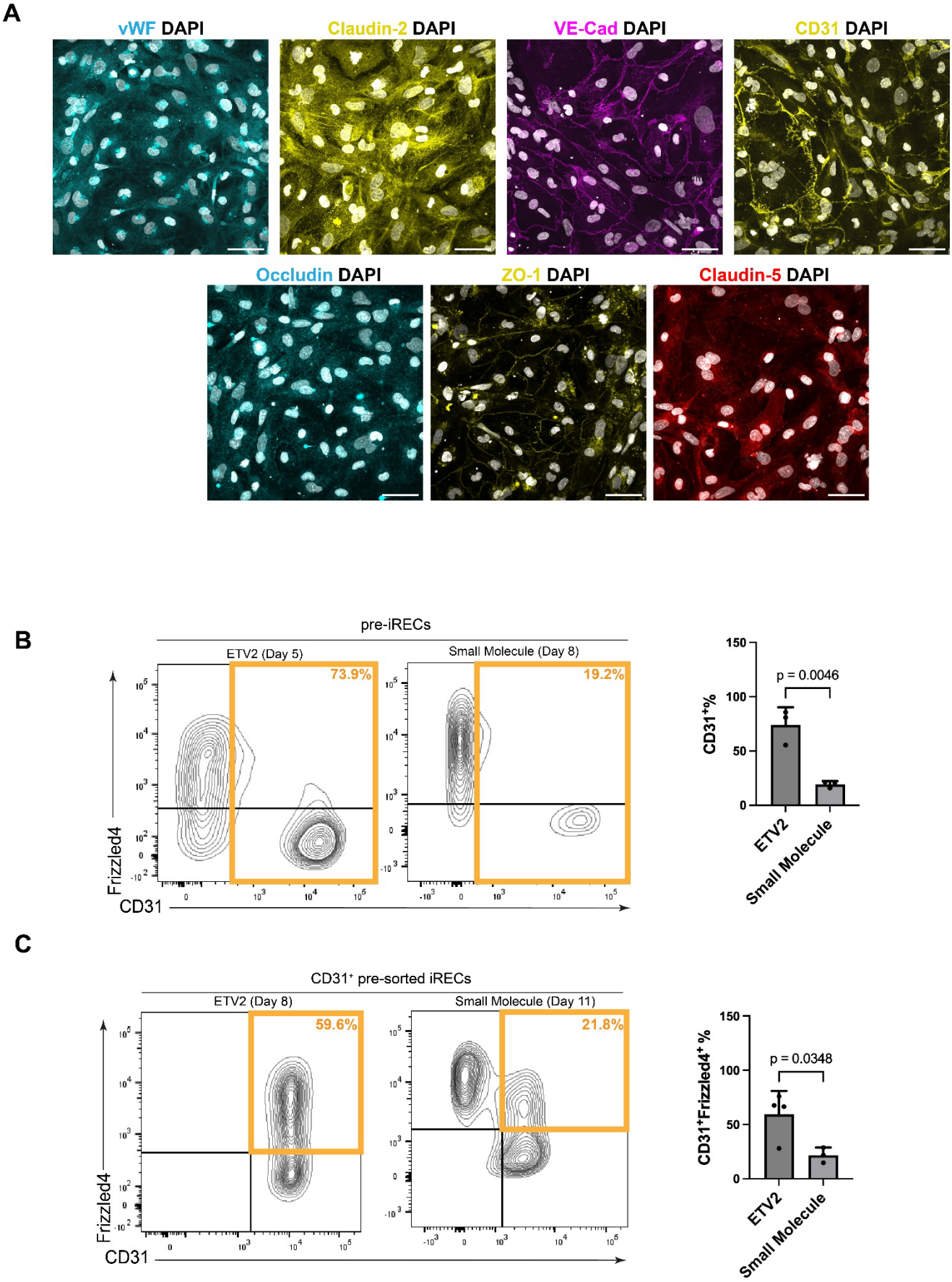

Supplementary fig 5. Differentiation of iRECs using the ETV2 induction versus small-molecule protocol.

(A) Representative immunofluorescence images of EC, junctional, and retinal markers on CD31⁺Fz4⁺ iRECs generated with the small-molecule protocol. vWF and Occludin (Cyan), Claudin-2, CD31, and ZO-1-GFP (yellow), VE-Cadherin (magenta), Claudin-5 (red), and all nuclei (White). Scale bars: 50 μm. (B) Representative flow cytometry analysis of pre-iRECs generated by ETV2 induction or small-molecule protocol (*left*) and corresponding quantification (*right*; N = 3 independent

biological replicates, n = 3 technical replicates). (C) Representative flow cytometry analysis of $CD31^+$ pre-sorted iRECs generated by ETV2 induction or small-molecule protocol (*left*) and corresponding quantification (*right*; N = 3 independent biological replicates, n = 3 technical replicates). All graphs represent means ± SD. Two-tailed unpaired Student t-tests were performed for all statistical comparisons. Significance levels were set at $p > 0.05$, $*p \leq 0.05$, $**p \leq 0.01$, $***p \leq 0.001$ and $****p \leq 0.0001$. All immunofluorescence staining experiments were performed once to confirm protein expression and ensure reproducibility.

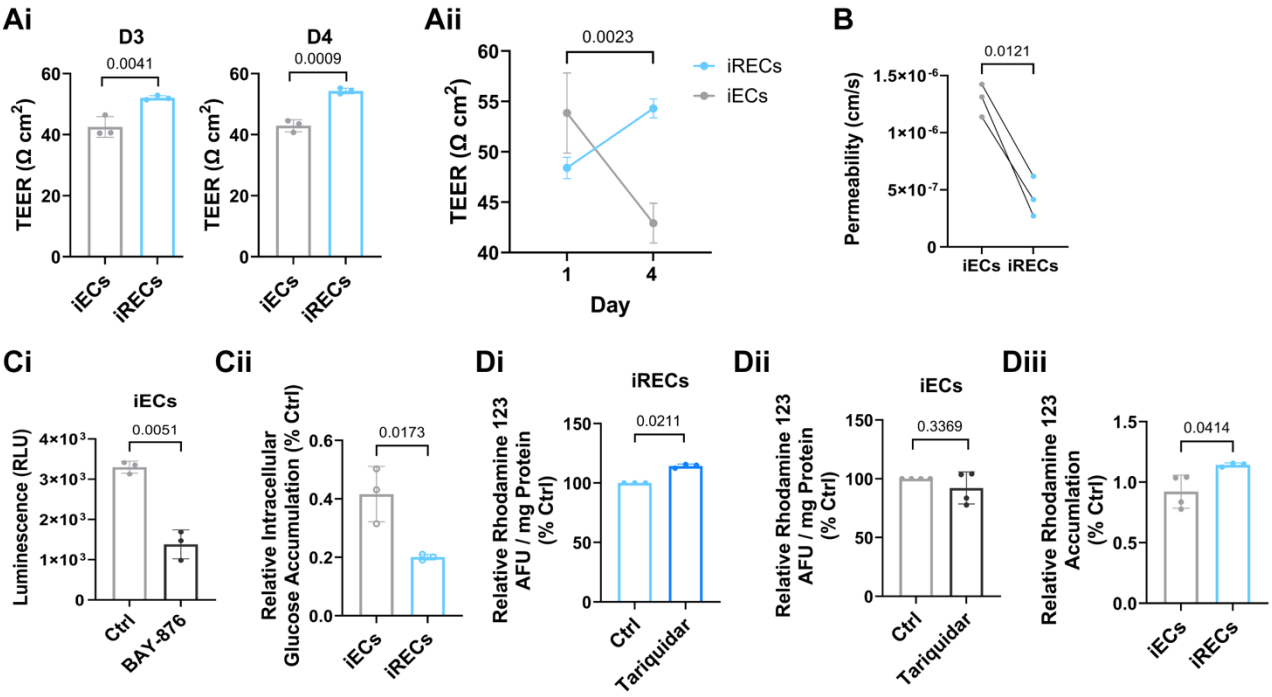

Supplementary fig 6. Barrier integrity and transporter activity in iECs and iRECs.
(A) i. Post-hoc Tukey's analysis of the iEC and iREC TEER data on day three and four. ii. Two-factor repeated measures ANOVA analysis comparing iREC and iEC TEER data at early (Day 1) and later time points (Day 4) to evaluate barrier properties over time (N = 3 independent biological replicates, n = 3 technical replicates). (B) Permeability assay for iECs and iRECs on day four (N = 3 independent biological replicates, n = 2 - 3 technical replicates). (C) i. GLUT1 uptake assay for iECs treated with or without the GLUT1 inhibitor, Bay-876 (N = 3 independent biological replicates, n = 3 technical replicates). Relative light unit (RLU) ii. Relative glucose uptake for iECs and iRECs compared to control (N = 3 independent biological replicates, n = 3 technical replicates). (D) i. P-gp uptake assay for iRECs treated with or without the p-gp inhibitor, Tariquidar. ii. P-gp uptake assay for iECs treated with or without the p-gp inhibitor, Tariquidar (N = 4 independent biological replicates, n = 2 - 3 technical replicates). iii. Relative Rhodamine 123 uptake for iECs and iRECs compared to control (N = 3 - 4 independent biological replicates, n = 2 - 3 technical replicates). All graphs represent means ± SD. Two-tailed paired Student t-tests were performed to statistically compare all permeability data. For TEER assays, we utilized two-factor repeated measures ANOVA to compare cell types. Post-hoc Tukey's tests were then performed to analyze individual days. Two-tailed unpaired Student t-tests were performed for all other statistical comparisons. Significance levels were set at $p > 0.05$, $*p \leq 0.05$, $**p \leq 0.01$, $***p \leq 0.001$ and $****p \leq 0.0001$.

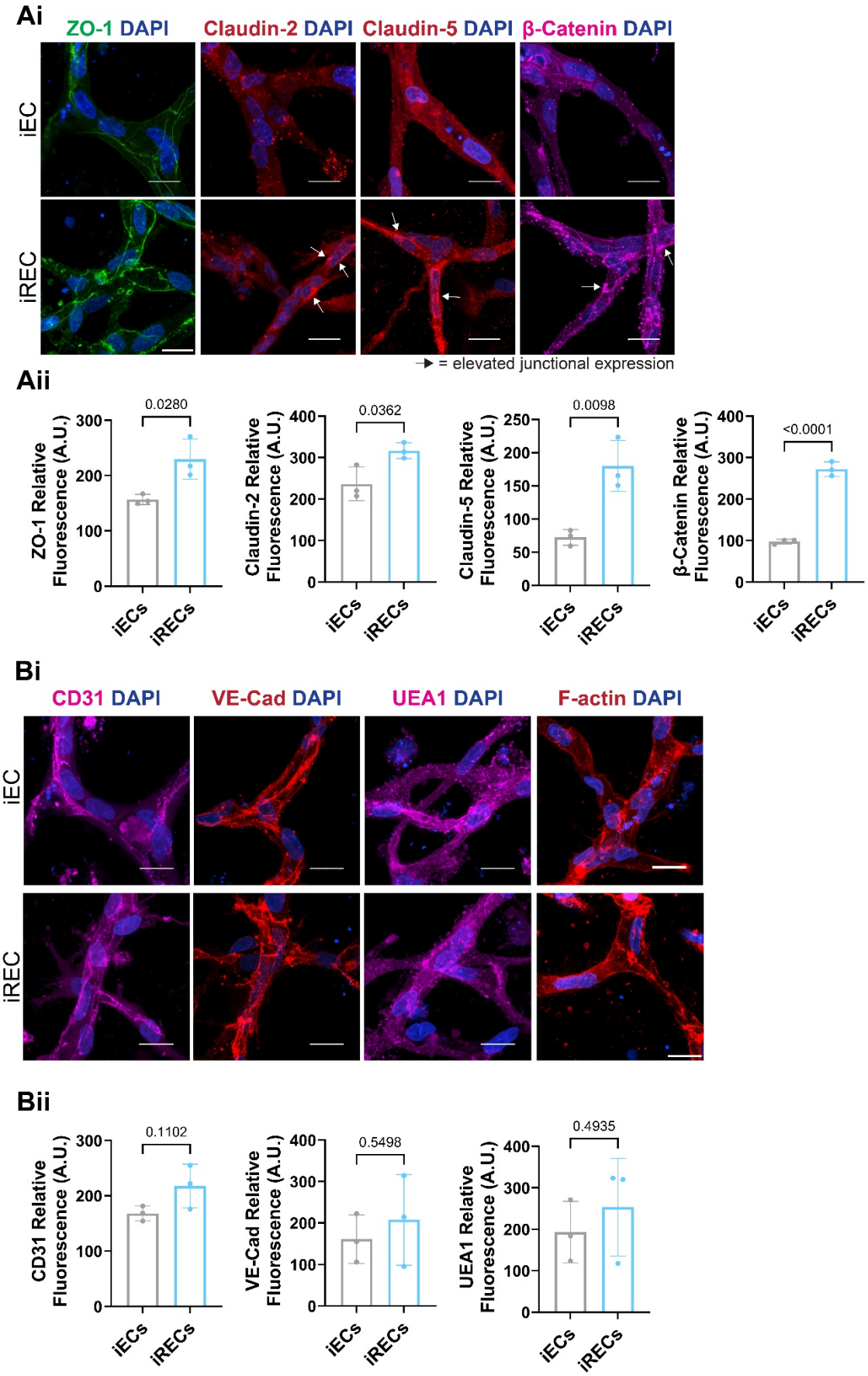

Supplementary fig 7. Junctional and endothelial marker expression in 3D iEC and iREC vascular networks.

(A) i. Representative immunofluorescence images of junctional protein expression. Arrows indicate elevated junctional expression in iRECs. ii. Quantification of relative fluorescence intensity in iECs and iRECs (N = 3 independent biological replicates, n = 3 technical replicates). (B) i. Representative immunofluorescence images of endothelial cell marker expression. ii. Quantification of relative fluorescence intensity in iECs and iRECs (N = 3 independent biological replicates, n = 3 technical

replicates). ZO-1-GFP (green), Claudin-2, Claudin-5, VE-Cadherin, and F-actin (red), β-catenin, CD31, and UEA1 (magenta), and nuclei (blue). Scale bars: 20 μm. All graphs represent means ± SD. Two-tailed unpaired Student t-tests were performed for all statistical comparisons. Significance levels were set at $p > 0.05$, $*p \leq 0.05$, $**p \leq 0.01$, $***p \leq 0.001$ and $****p \leq 0.0001$. All immunofluorescence staining experiments were performed with three independent biological replicates to accurately quantify associated fluorescence expression and ensure reproducibility.

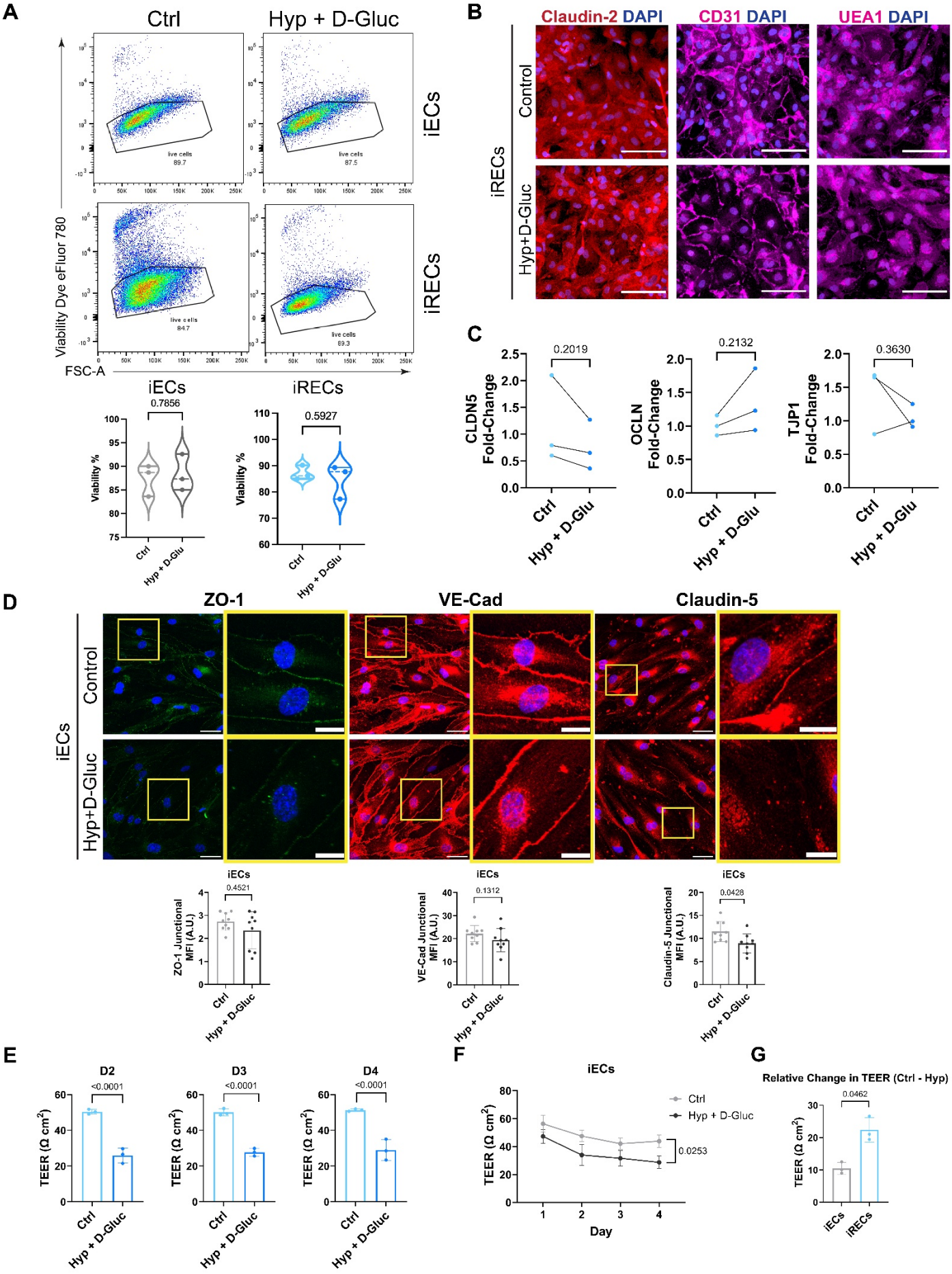
A
Ctrl
Hyp + D-Gluc
iECs
iRECs
Viability Dye eFluor 780
FSC-A
live cells
89.7
87.5
84.7
89.3
iECs
iRECs
0.7856
0.5927
Viability %
Ctrl
Hyp + D-Glu
B
Claudin-2 DAPI
CD31 DAPI
UEA1 DAPI
Control
Hyp+D-Gluc
C
CLDN5 Fold-Change
OCLN Fold-Change
TJP1 Fold-Change
0.2019
0.2132
0.3630
D
ZO-1
VE-Cad
Claudin-5
Control
Hyp+D-Gluc
iECs
ZO-1 Junctional MFI (A.U.)
VE-Cad Junctional MFI (A.U.)
Claudin-5 Junctional MFI (A.U.)
0.4521
0.1312
0.0428
E
D2
D3
D4
<0.0001
TEER (Ω cm²)
F
iECs
Ctrl
Hyp + D-Gluc
0.0253
Day
G
Relative Change in TEER (Ctrl - Hyp)
0.0462

Supplementary fig 8. Impact of DR conditions on iEC and iREC viability, protein and gene expression, and barrier function.
(A) Cell viability analysis of control and diabetic-treated iECs and iRECs (N = 3 independent biological replicates, n = 3 technical replicates). (*Top*) Representative flow cytometry images. (*Bottom*) Quantification of flow cytometry results. (B) Representative immunofluorescence images of iRECs with or without diabetic treatment (Hyp + D-Gluc). Claudin-2 (red), CD31 and UEA1 (magenta), and nuclei (blue). Scale bars: 100 μm. (C) RT-qPCR analysis for Claudin-5 (CLDN5), Occludin (OCLN), and ZO-1 (TJP1) within iRECs exposed to diabetic or control conditions (N = 3 independent biological replicates, n = 3 technical replicates). (D) (*Top*) Representative immunofluorescence images of junctional protein markers on iECs in control or diabetic retinopathy conditions. ZO-1-GFP (green), VE-Cad and Claudin-5 (red), and nuclei (blue). Scale bars: 50 μm (originals) and 20 μm (insets). (*Bottom*) Corresponding quantification of mean fluorescent intensity at cell-cell junctions (N = 3 independent biological replicates, n = 3 technical replicates). (E) Post-hoc Tukey's analysis of DR iREC TEER data on day two, three, and four (N = 3 independent biological replicates, n = 3 technical replicates). (F) TEER measurements of iECs under control or diabetic conditions (N = 3 independent biological replicates, n = 2 - 3 technical replicates). (G) Relative change in TEER in iECs and iRECs on day three (N = 3 independent biological replicates, n = 2 - 3 technical replicates). All graphs represent means ± SD. Two-tailed paired Student t-tests were performed to statistically compare all diabetic retinopathy and qPCR data. For TEER assays, we utilized two-factor repeated measures ANOVA to compare cell types. Post-hoc Tukey's tests were then performed to analyze individual days. Two-tailed unpaired Student t-tests were performed for all other statistical comparisons. Significance levels were set at $p > 0.05$, $*p \leq 0.05$, $**p \leq 0.01$, $***p \leq 0.001$ and $****p \leq 0.0001$. Fig. D immunofluorescence staining experiments were performed with three independent biological replicates to accurately quantify associated fluorescence expression and morphology and ensure reproducibility. Fig. B immunofluorescence staining experiments were performed once to confirm protein expression and validate reproducibility of previous independent experiments.

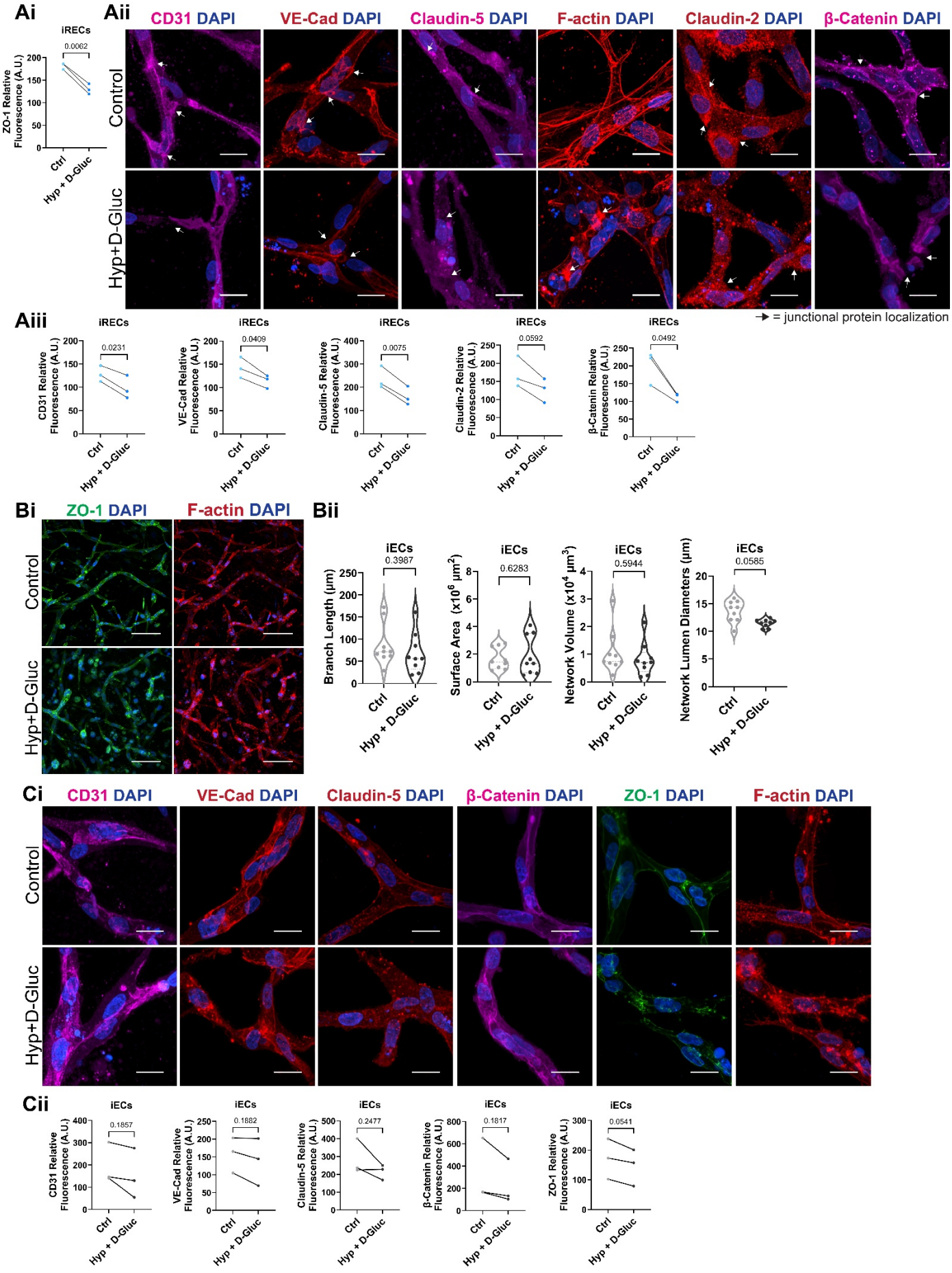

Supplementary fig 9. 3D iREC and iEC vascular network phenotype and morphology in healthy and diabetic conditions.

(A) i. Quantification of relative ZO-1 fluorescence intensity for iREC vascular networks with or without diabetic treatment (N = 3 independent biological replicates, n = 3 technical replicates). ii. Representative immunofluorescence images of endothelial cell, junctional, and retinal protein

markers on 3D iREC vascular networks with or without diabetic treatment. Arrows indicate protein localization at cell-cell junctions. CD31, Claudin-5, and β-catenin (magenta), VE-Cad, F-actin, and Claudin-2 (red), and nuclei (blue). Scale bars: 20 μm. iii. Quantification of relative fluorescence intensity for iREC vascular networks with or without diabetic treatment (N = 3 independent biological replicates, n = 3 technical replicates). (B) i. Representative F-actin and ZO-1 immunofluorescence images of 3D iEC vascular networks with or without diabetic retinopathy treatment. ZO-1-GFP (green), F-actin (red), and nuclei (blue). Scale bars: 100 μm. ii. Quantification of 3D iEC vascular network branch lengths, surface areas, network volumes, and lumen diameters for networks with or without diabetic treatment (N = 3 independent biological replicates, n = 3 technical replicates). (C) i. Representative immunofluorescence images of endothelial cell and junctional protein markers on 3D iEC vascular networks with or without diabetic treatment. CD31 and β-catenin (magenta), VE-Cad, Claudin-5, and F-actin (red), ZO1-GFP (green), and nuclei (blue). Scale bars: 20 μm. ii. Quantification of relative fluorescence intensity for iEC vascular networks with or without diabetic treatment (N = 3 independent biological replicates, n = 2 - 3 technical replicates). All graphs represent means ± SD. Two-tailed paired Student t-tests were performed to statistically compare all protein fluorescence data. Two-tailed unpaired Student t-tests were performed for all morphology comparisons. Significance levels were set at $p > 0.05$, $^{*}p \leq 0.05$, $^{**}p \leq 0.01$, $^{***}p \leq 0.001$ and $^{****}p \leq 0.0001$. All immunofluorescence staining experiments were performed with three independent biological replicates to accurately quantify associated fluorescence expression and morphology and ensure reproducibility.

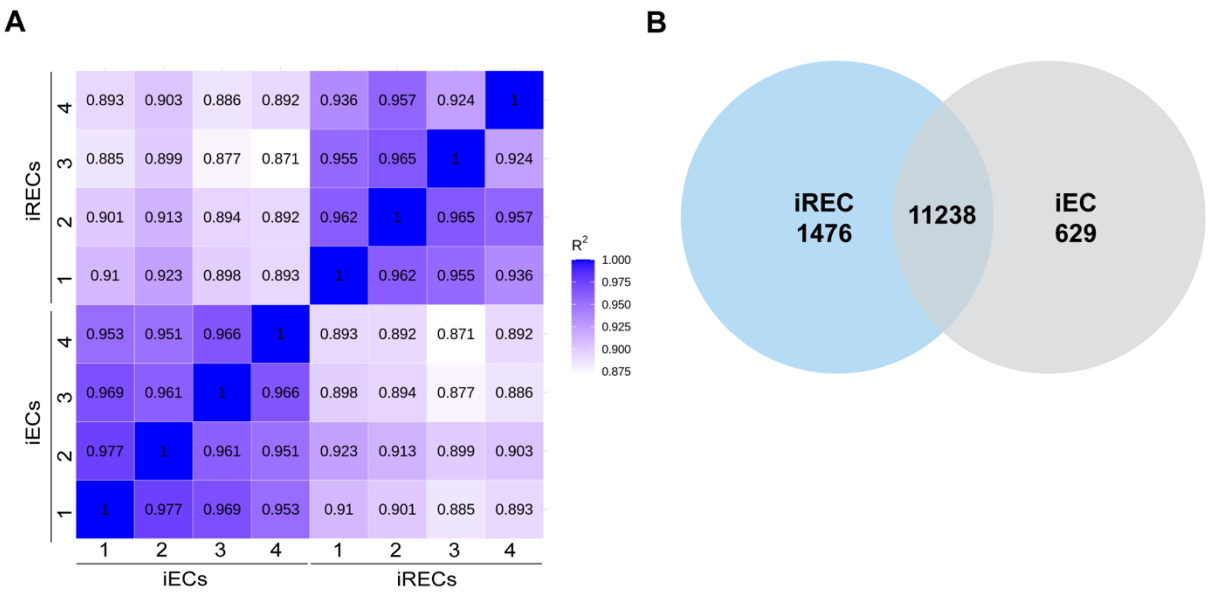

Supplementary fig 10. Bulk RNA-Seq analysis of iECs and iRECs.
(A) Correlation analysis and (B) Venn diagram illustrating the differential gene expression between iECs and iRECs across four biological replicates.

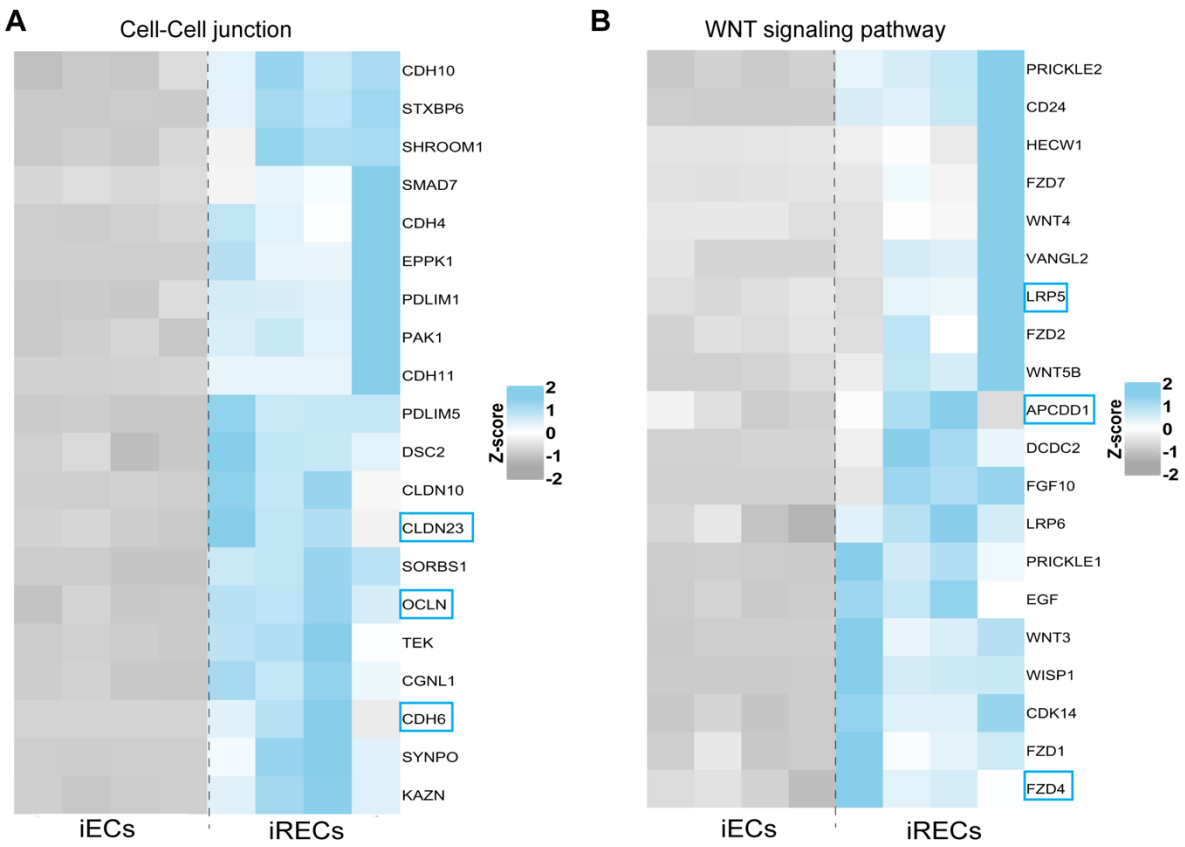

Supplementary fig 11. Bulk RNA-Seq analysis of iECs and iRECs.
Heatmap analysis of (A) cell-cell junction-related genes and (B) Wnt signaling pathway-related genes in iECs and iRECs across four biological replicates.

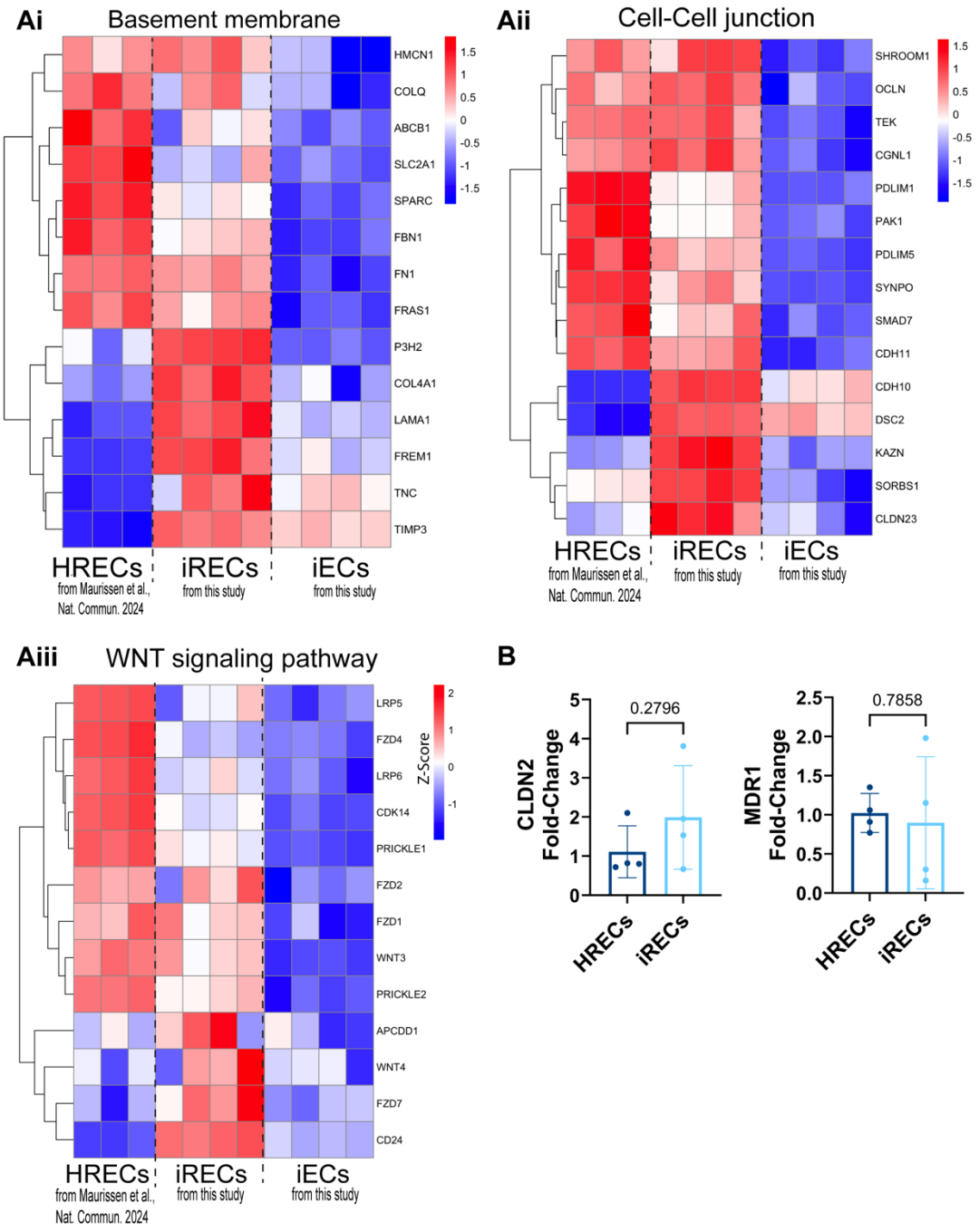

Supplementary fig 12. Heat map and RT-qPCR analysis of retinal genes in HRECs, iRECs, and iECs.

(A) Heat map analysis of i. basement membrane-, ii. cell-cell junction-, and iii. Wnt signaling pathway-related genes in HRECs, iRECs, and iECs. (B) RT-qPCR analysis of Claudin-2 (*CLDN2*) and p-gp (*MDR1*) gene expression within HRECs and iRECs. N = 4 independent biological replicates, n = 3 technical replicates for each gene. All graphs represent means ± SD. Two-tailed unpaired Student t-tests were performed for all statistical comparisons. Significance levels were set at $p > 0.05$, $*p \leq 0.05$, $**p \leq 0.01$, $***p \leq 0.001$ and $****p \leq 0.0001$.

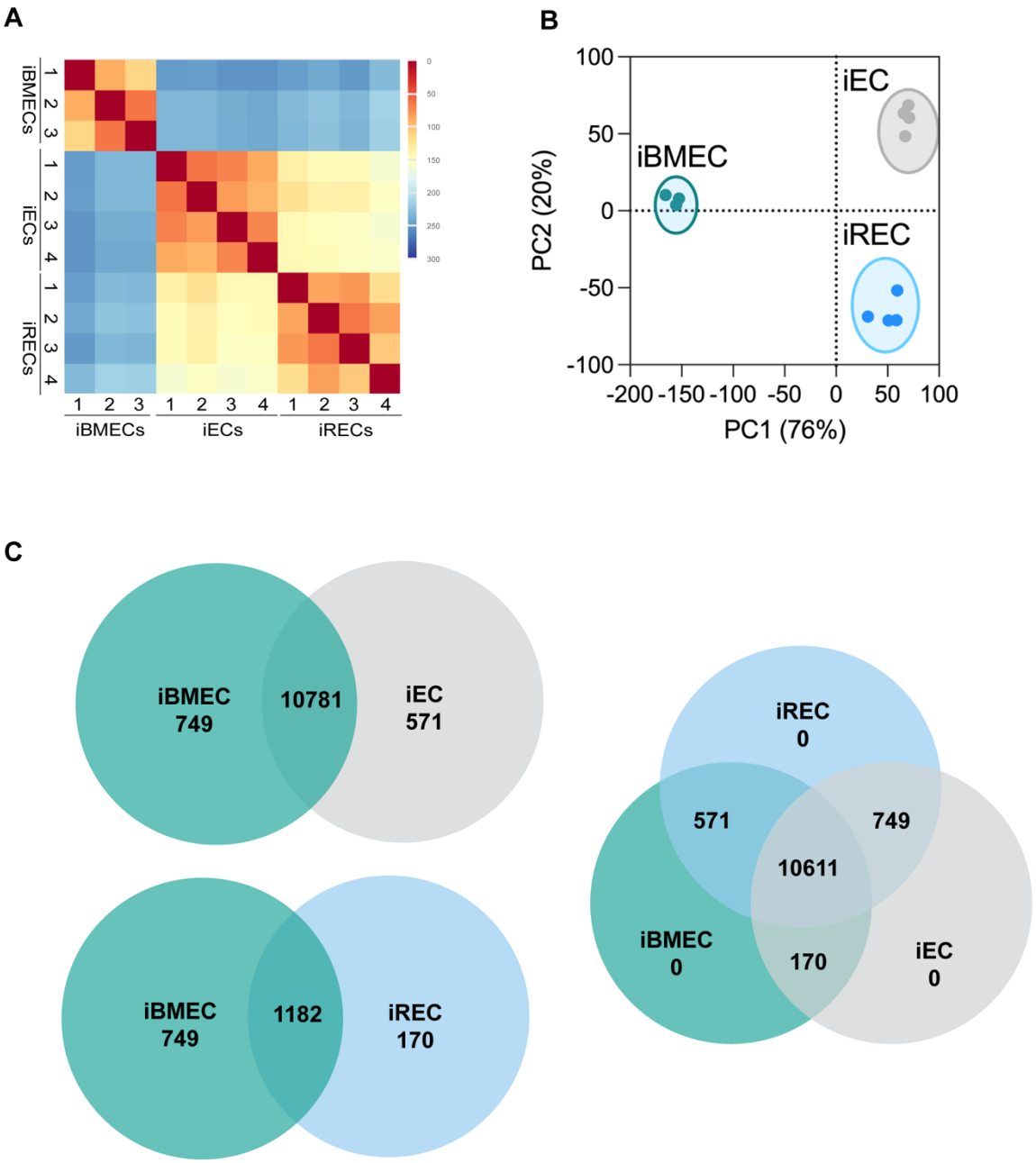

Supplementary fig 13. Bulk RNA-Seq analysis of iECs, iRECs and iPSC-derived brain ECs (iBMECs).
(A) Correlation analysis of iECs, iRECs and iBMEC across three or four biological replicates. (B) Principal component analysis of RNA-Seq data from iECs, iRECs, and iBMECs. (C) Venn diagram illustrating the differential gene expression between iECs, iRECs, and iBMECs.

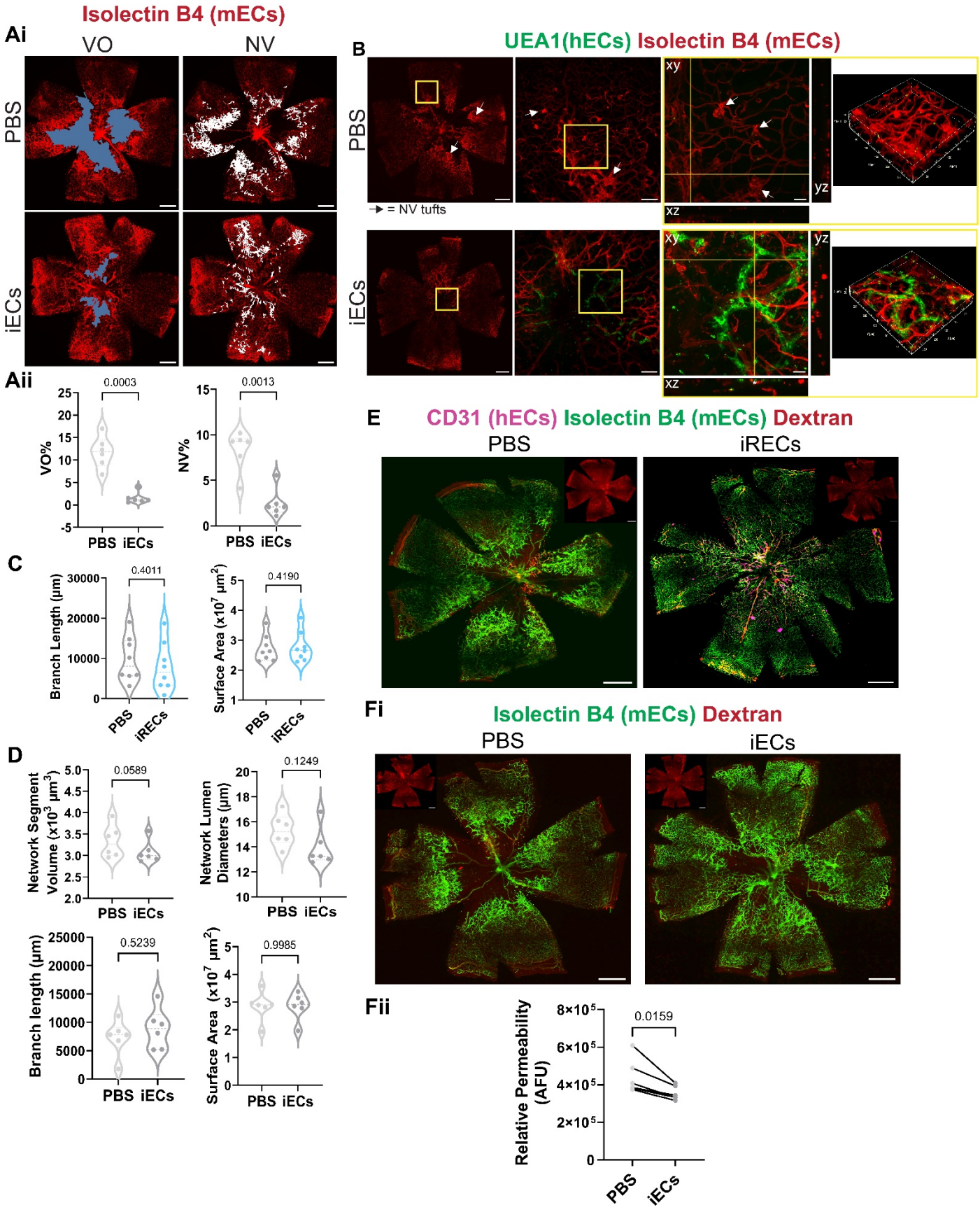

Supplementary fig 14. PBS, iEC, and iREC intravitreal injections in the OIR mouse model. (A) i. Representative immunofluorescence images of the OIR mouse retinal tissue at postnatal day 17 (P17), five days after intravitreal injection of PBS or iECs. Isolectin B4 (red), vaso-obliteration (VO) area (blue), and neovascularization (NV) area (white). Scale bars: 500 µm. ii. Quantification of VO and NV at P17 (n = 6). (B) Representative immunofluorescence images of whole mount retina, cross-sections of the OIR mouse retinal tissue, and 3D reconstructions of mouse vascular regions at P17 for PBS (*top*) and iEC (*bottom*). Isolectin B4 (red) and UEA1 (green). Arrows depict pathological neovascular tufts and yellow crosshairs demonstrate location of xz and yz planes. Scale

bars: 500 μm, 100 μm, and 25 μm, (left to right). (C) Quantification of branch length and surface area of retinas injected with PBS or iRECs. All quantifications are n = 8. (D) Quantification of segment volume, lumen diameter, branch length, and surface area of retinas injected with PBS or iECs. All quantifications are n = 6. (E) Representative immunofluorescence images of PBS or iREC-treated mouse retina injected with rhodamine dextran (red). Isolectin B4 (green) and hCD31(magenta). Scale bars: 500 μm. (F) i. Representative immunofluorescence images of PBS or iEC-treated mouse retina injected with rhodamine dextran (red). Isolectin B4 (green). Scale bars: 500 μm. ii. Quantification of fluorescence intensity of 70 kDa rhodamine dextran extracted from OIR retinas (n = 6). All n refers to biologically independent mice. Contralateral eyes from the same pups received different treatments. One eye received cellular treatment and the contralateral eye received PBS treatment. All graphs represent means ± SD. Two-tailed paired Student t-tests were performed to statistically compare all data. Significance levels were set at $p > 0.05$, $*p \leq 0.05$, $**p \leq 0.01$, $***p \leq 0.001$ and $****p \leq 0.0001$. All Fig. A – B immunofluorescence staining experiments were performed with six independent biological replicates and Fig. E - F immunofluorescence staining experiments were performed with two independent biological replicates to confirm network morphology, integration, and perfusability and ensure reproducibility.

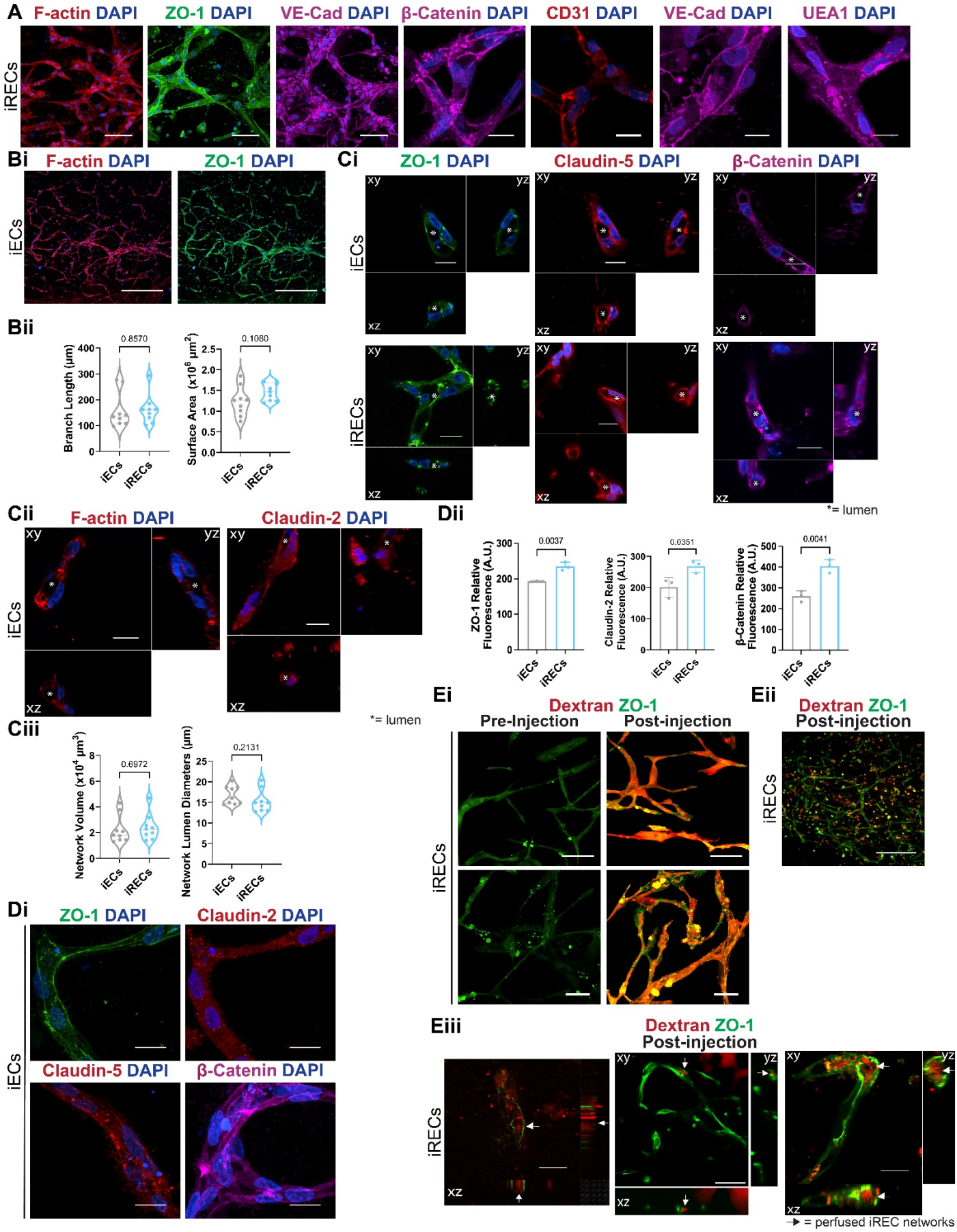

Supplementary fig 15. Characterization of iBRB-on-a-chip.
(A) Representative immunofluorescence images of 3D iREC vascular networks. F-actin and CD31 (red), ZO-1-GFP (green), VE-Cadherin, β-catenin, and UEA1 (magenta), and nuclei (blue). Scale bars: 100 μm (left three) and 20 μm (right four). (B) i. Representative immunofluorescence images of 3D iEC vascular networks within the MPS. F-actin (red), ZO-1 (green), and nuclei (blue). Scale bars: 500 μm. ii. Quantification of 3D iEC and iREC vascular network branch lengths and surface

areas (N = 3 independent biological replicates, n = 3 technical replicates). (C) i. Representative immunofluorescence cross-sectional images of 3D iREC and iEC vascular networks within the MPS showing vessel lumens (asterisks). ZO-1-GFP (green), Claudin-5 (red), β-catenin (magenta), and nuclei (blue). Scale bars: 20 μm. ii. Representative immunofluorescence cross-sectional images of 3D iEC vascular networks within the MPS showing vessel lumens (asterisks). F-actin and Claudin-2 (red) and nuclei (blue). Scale bars: 20 μm. iii. Quantification of 3D iEC and iREC vascular network volumes and lumen diameters (N = 3 independent biological replicates, n = 3 technical replicates). (D) i. Representative immunofluorescence images of 3D iEC vascular networks within the MPS. ZO-1-GFP (green), Claudin-2 and Claudin-5 (red), β-catenin (magenta), and nuclei (blue). Scale bars: 20 μm. ii. Quantification of relative fluorescence intensity of junctional proteins on iEC and iEC vascular networks within the MPS (N = 3 independent biological replicates, n = 3 technical replicates). (E) i. Representative immunofluorescence images of the 3D iREC networks before (*left*) and after (*right*) 70 kDa rhodamine dextran injection. ZO-1-GFP (green) and rhodamine dextran (red). Scale bars: 100 μm (top panel) and 50 μm (bottom panel). ii. Representative immunofluorescence image of the 3D iREC networks after 70 kDa rhodamine dextran injection. ZO-1-GFP (green) and rhodamine dextran (red). Scale bar: 250 μm. iii. Cross-sectional images of 3D iREC networks perfused by 70 kDa rhodamine dextran after injection. ZO-1-GFP (green) and rhodamine dextran (red). Arrows depict iREC networks and lumina perfused with rhodamine dextran. Scale bars: 100 μm (middle) and 20 μm (left and right). All graphs represent means ± SD. Two-tailed unpaired Student t-tests were performed for all statistical comparisons. Significance levels were set at $p > 0.05$, $^{*}p \leq 0.05$, $^{**}p \leq 0.01$, $^{***}p \leq 0.001$ and $^{****}p \leq 0.0001$. Fig. A immunofluorescence staining experiments were performed once to confirm protein expression and validate reproducibility of previous independent experiments. All other immunofluorescence staining experiments were performed with three independent biological replicates to accurately quantify associated fluorescence expression and morphology and ensure reproducibility.

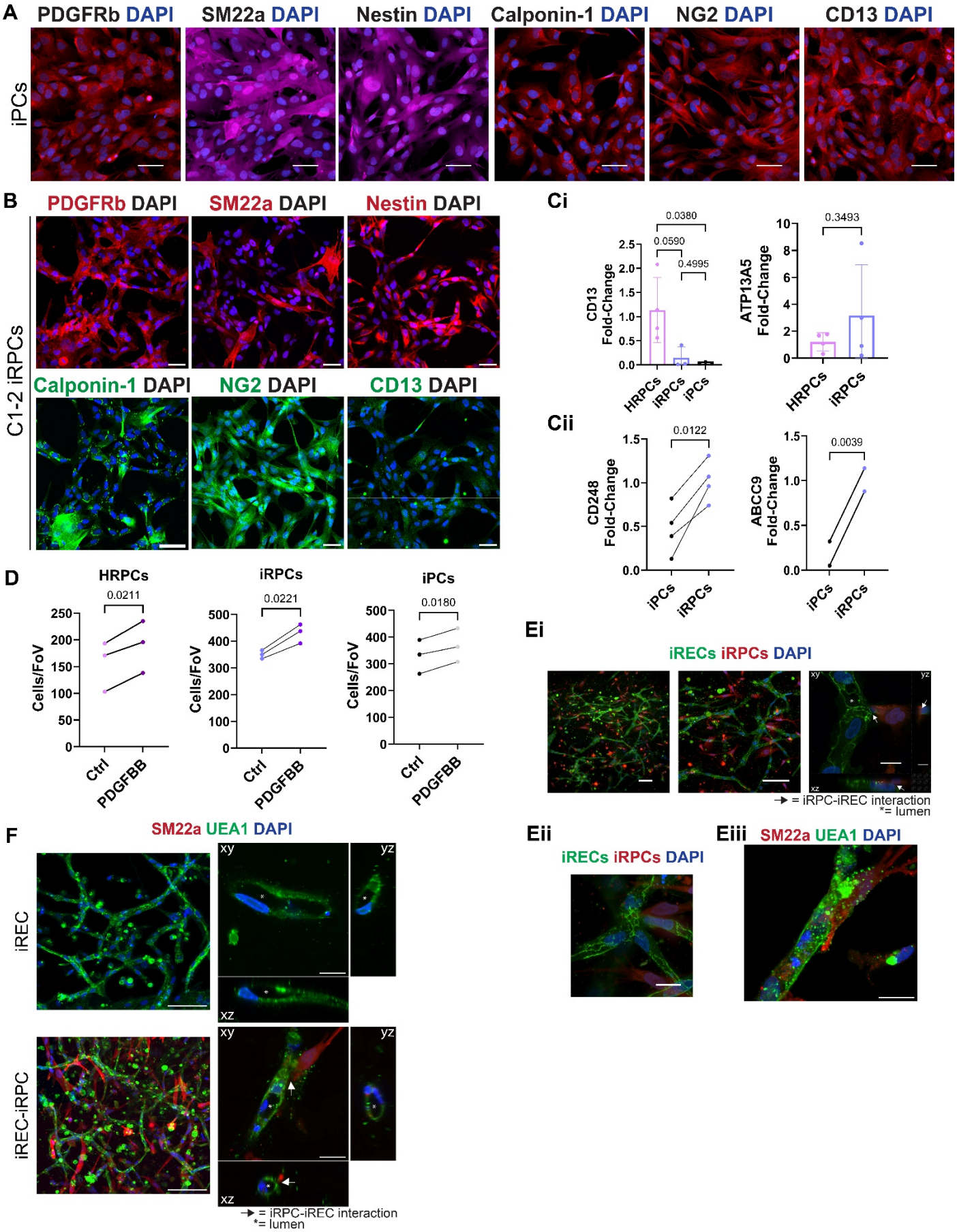

Supplementary fig 16. Characterization of iRPCs and iREC-iRPC iBRB-on-a-chip.
(A) Representative immunofluorescence images of pericyte markers in iPCs. PDGFRβ, Calponin-1, NG2, and CD13 (red), SM22α and Nestin (magenta), and nuclei (blue). Scale bars: 50 μm. (B) Representative immunofluorescence images of pericyte markers in C1-2-derived iRPCs. PDGFRβ, SM22α, and Nestin (red), Calponin-1, NG2, and CD13 (green), and nuclei (blue). Scale bars: 50 μm.

(C) i. RT-qPCR analysis of HRPCs, iRPCs and iPCs. CD13 (N = 3 – 4 independent biological replicates); ATP13A5 (N = 4 independent biological replcates) ii. RT-qPCR analysis of CD248 (N = 4 independent biological replicates) and ABCC9 (N = 2 independent biological replicates) expression within iRPCs and iPCs. (D) Quantification of Transwell migration assay of HRPCs, iRPCs, and iPCs (N = 3 independent biological replicates, n = 2 - 3 technical replicates). (E) i-iii. Representative immunofluorescence images of the iREC-iRPC co-cultured iBRB-on-chip displaying perivascular iRPCs surrounding and encapsulating iREC networks in order to support their functional lumens. Asterisks denote examples of lumens and arrows highlight iRPC-iREC interactions. iRECs (ZO1-GFP), iRPCs (red cell tracker), SM22α (red), UEA1 (green), and nuclei (blue). Scale bars: 100 μm (Ei left and middle), 20 μm (Ei xy plane in the right panel, Eii, and Eiii), and 10 μm (Ei xz and yz planes in the right panel). (F) Representative immunofluorescence images and cross-sectional views of iREC and iREC-iRPC networks. Asterisks denote examples of lumens, and arrows highlight iRPC-iREC interactions. SM22α (red), UEA1 (green), and nuclei (blue). Scale bars: 100 μm (left panel) and 20 μm (right panel). All graphs represent means ± SD. Two-tailed paired Student t-tests were performed to statistically compare Fig. Cii and D data. A one-factor ANOVA was used to statistically compare the *CD13* qPCR data. Post-hoc Tukey's tests were performed to analyze multiple comparisons. Two-tailed unpaired Student t-tests were performed for the *ATP13A5* qPCR data. Significance levels were set at $p > 0.05$, $^{*}p \leq 0.05$, $^{**}p \leq 0.01$, $^{***}p \leq 0.001$ and $^{****}p \leq 0.0001$. Fig. F immunofluorescence staining experiments were performed with three independent biological replicates to accurately quantify associated fluorescence expression and morphology and ensure reproducibility. All other immunofluorescence staining experiments were performed once to confirm protein expression and validate reproducibility of previous independent experiments.

Supplementary table 1. Key Resources.

Antibody	Vendor	Cat. No.	Application	Species	Dilution
Calponin-1	SCBT	sc-58707	ICC	Mouse	1/100
PDGFRb	SCBT	sc-432	ICC	Rabbit	1/200
CD13	SCBT	sc-18899	ICC	Mouse	1/100
Nestin	SCBT	NB300-265s	ICC	Rabbit	1/200
NG2	SCBT	sc-166251	ICC	Mouse	1/100
Transgelin (SM22α)	Cell Signaling	40471s	ICC	Rabbit	1/100
CD31	Abcam	ab28364	ICC	Rabbit	1/100
VE-Cadherin	SCBT	sc-9989	ICC	Mouse	1/100 or 1/4000
von Willebrand Factor	SCBT	sc-365712	ICC	Mouse	1/100
Alexa Fluor 546 Phalloidin	Thermo Fisher	A22283	ICC	N/A	1/400
Occludin	Thermo Fisher Scientific	711500	ICC	Rabbit	1/100
Claudin-5	Thermo Fisher Scientific	35-250-0	ICC	Mouse	1/50; 1/200
ZO-1	Thermo Fisher Scientific	40-2200	ICC	Rabbit	1/100
Claudin-2	Thermo Fisher Scientific	710221; 5600	ICC	Rabbit; Mouse	1/200; 1/100
β-catenin	SCBT	sc-7199; sc-393501	ICC	Rabbit; Mouse	1/100
Dylight-conjugated Ulex Europaeus Agglutinin	Vector Laboratories	DL-1068-1	ICC	N/A	1/400
DAPI	Thermo Fisher Scientific	D1306	ICC	N/A	1/1000
ICAM-1	R&D systems	BBA3	ICC	Mouse	1/100
In vivo					
Griffonia Simplicifolia Lectin I (GSL I) Isolectin B4, DyLight™ 594	Vector Laboratories	DL-1207-.5	IF	N/A	1/400
Anti-NG2, Alexa Fluor™488 Conjugate Antibody	Millipore Sigma	AB5320A4	IF	Rabbit	1/200
Rhodamine-conjugated Ulex Europaeus Agglutinin	Vector Laboratories	RL-1062-2	IF	N/A	1/400
Flow cytometry					
PE-Anti-Human CD140b	BD Pharmingen	558821	Flow cytometry	Mouse	1/10
APC-Anti-Human CD344	Miltenyi Biotec	130-106-614	Flow cytometry	Mouse	1/10
PE-Anti-Human CD31	BD Pharmingen	555446	Flow cytometry	Mouse	1/10
eBioscience Fixable Viability Dye eFluor 780	Invitrogen	65-0865-14	Flow cytometry		1/1000
Western Blot					
P16-INK4A	proteintech	10883-1-AP	WB	Rabbit	1/1000
P21 Waf1/Cip1	Cell Signaling	2947S	WB	Rabbit	1/1000

β-actin	Cell Signaling	3700S	WB	Mouse	1/4000
Anti-mouse IgG, HRP-linked	Cell Signaling	7076P2	WB	Horse	1/2000
Anti-rabbit IgG, HRP-linked	Cell Signaling	7074P2	WB	Horse	1/2000
Primers	**Taqman assay**				
Claudin-5	Hs00533949_s1				
Lrp5	Hs00182031_m1				
ZO-1	Hs01551861_m1				
Occludin	Hs00170162_m1				
TBP	Hs00427620_m1				
Primers	**SYBR Green**				
CD13	Fw: GACCAAAGTAAAGC GTGGAATCG	Rev: TCTCAGCGTCAC CCGGTAG			
ATP13A5	Fw: GGTTCCCGGAGACA TTCTTATT	Rev: GTCAAAGCACAC GAGGTTTATTT			
CD248	Fw: AGTGTTATTGTAGCGA GGGACA	Rev: CCTCTGGGAAGC TCGGTCTA			
ABCC9	Fw: CCAGCCGTGATGG GATTCG	Rev: GGCCATTACCCA ATACAGGAAC			
FZD4	Fw: CCTCGGCTACAACGT GACC	Rev: TGCACATTGGCA CATAAACAGA			
IGF2	Fw: GTGGCATCGTTGAGG AGTG	Rev: CACGTCCCTCTC GGACTTG			
CLDN2	Fw: CGGGACTTCTACTCAC CACTG	Rev: GGATGATTCCAG CTATCAGGGA			
CLDN5	Fw: CTCTGCTGGTTCGCC AACAT	Rev: CAGCTCGTACTT CTGCGACA			
CLDN10	Fw: GCATGTAGAGGACTTA TGATCGC	Rev: TCCGACTTTGGT ACACTTCATTC			
CLDN23	Fw: TCGAGGGCATGCAAG AGTTT	Rev: GGCGTCCAAAG GGTGGAATA			

Upcropped and unprocessed membrane

ß-actin

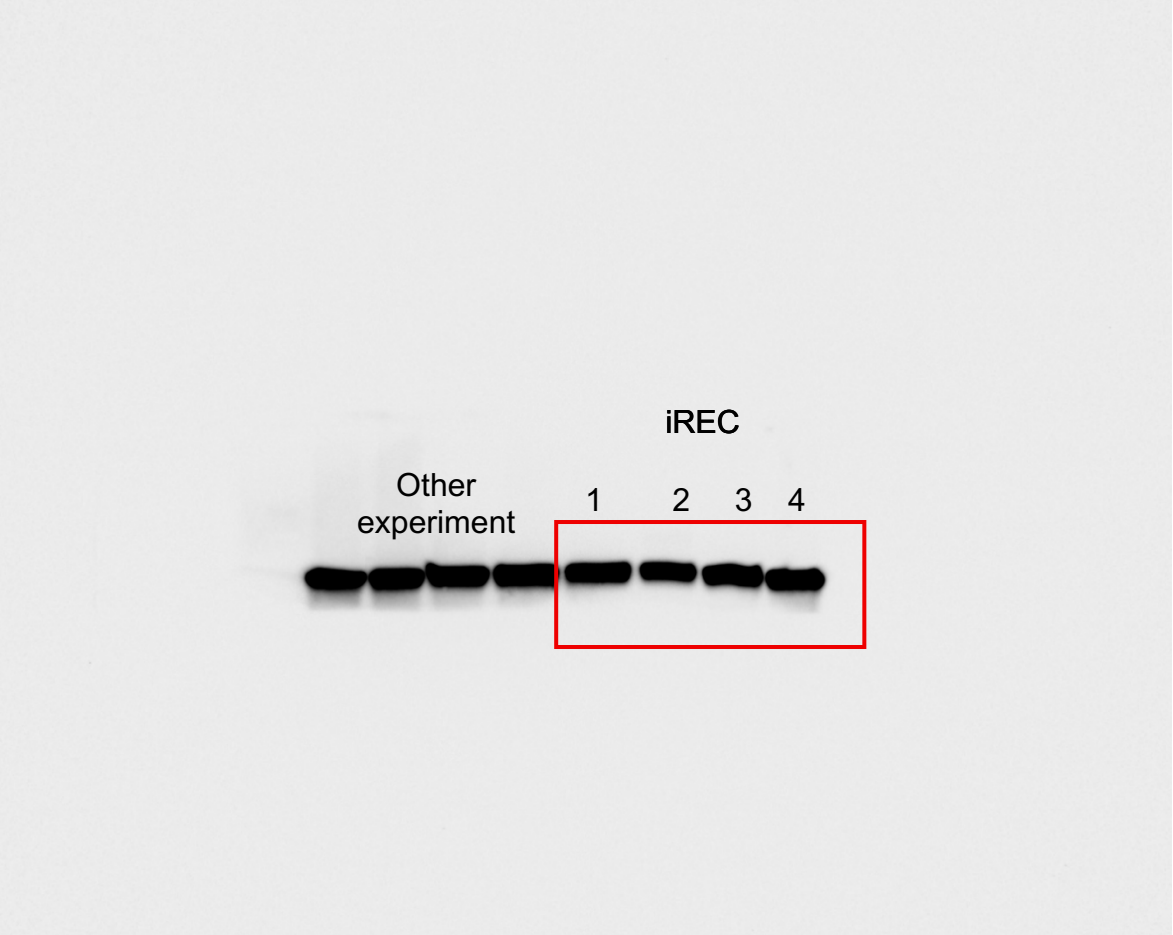

Blot with makers

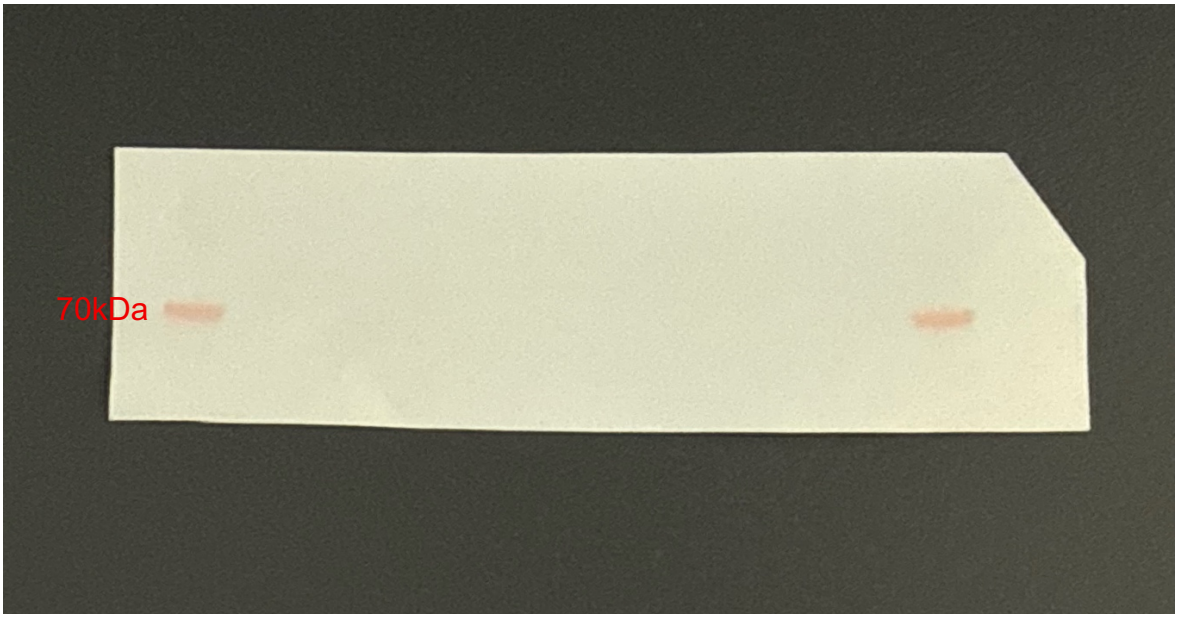

P16

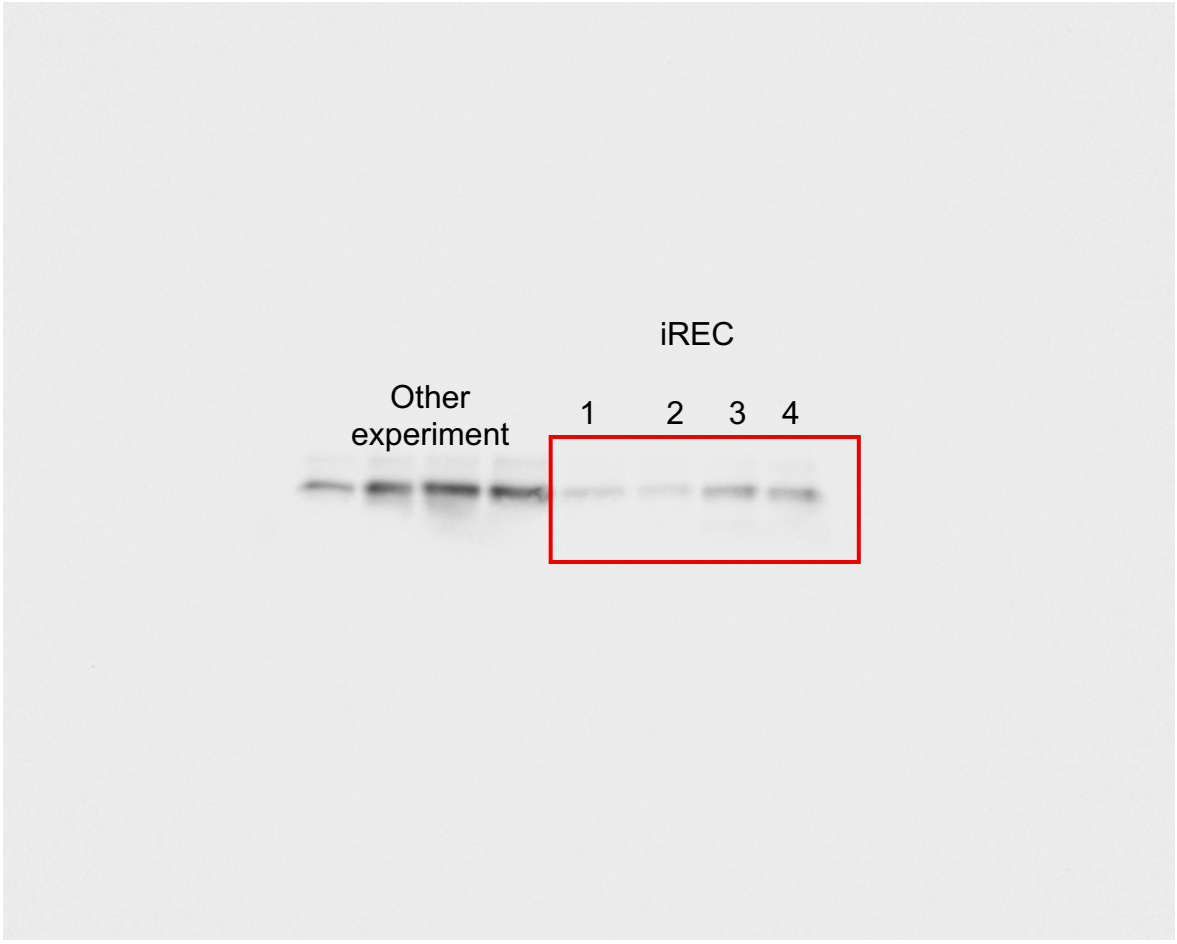

P21

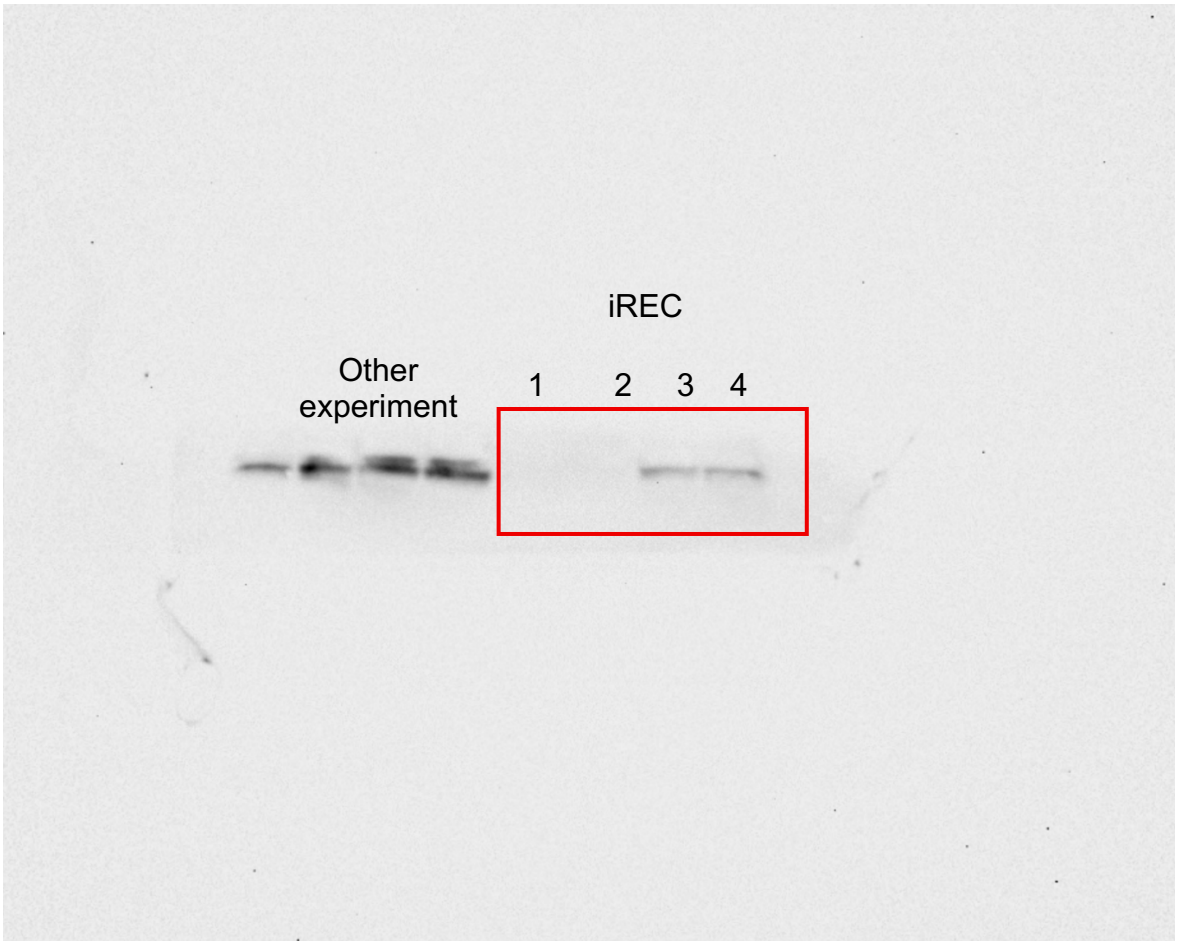

*P16 and P21 were run on the same blot and underwent one round of stripping before re-probing

Blot with makers